Journal of Thermal Analysis and Calorimetry, Vol. 91 (2008) 1, 29–35

THERMAL ANALYSIS OF Al–Cu–Mg–Si ALLOY WITH Ag/Zr ADDITIONS

Paola Bassani[1*], *E. Gariboldi*[2] *and D. Ripamonti*[2]

[1]CNR IENI, Lecco, C.so Promessi Sposi 29, 23900 LC, Italy
[2]Politecnico di Milano, Dipartimento di Meccanica, Milano, Italy

Heat-treatable aluminium alloys are widely used for structural applications. Their strength is obtained through age hardening phenomena, that are sensitive to microalloying.

In the present paper the results of thermal analyses on the ageing behaviour of an Al–Cu–Mg–Si alloy with silver and zirconium additions are presented. Specimens were water quenched after solution heat treatment, then aged at 453 K and a hardness-versus-time plot was drawn. Samples representative of different ageing conditions were subjected to DSC scans.

Peaks were identified taking into account θ and Q phases precipitation sequences. Solution treated samples showed GP/θ″/θ′/Q sequence, while in peak aged condition GP and θ″ precipitation peaks disappeared and a reduction of θ′ peak area was observed, witnessing the concurrent presence of θ″ and θ′ phases at peak hardness condition. Experimental data were compared with results from analogous investigations performed on a conventional commercial Al–Cu–Mg–Si alloy.

Keywords: *ageing behaviour, Al–Cu–Mg–Si alloy, silver addition*

Introduction

Heat treatable aluminium alloys are a widely used class of structural materials. Their low specific mass, together with a relatively high strength, makes them suitable for aircraft applications [1]. These alloys are usually serviced in the so-called T6 condition [2], that is gained by performing artificial ageing at peak hardness after a solution treatment. Among heat treatable alloys, high-strength alloys of the Al–Cu and Al–Cu–Mg systems (2xxx series), are of great interest when good creep properties are needed [3]. During ageing, these alloys show hardening phenomena thanks to the precipitation of inter-metallic non-equilibrium phases (age-hardening). Precipitation sequence of Al–Cu and Al–Cu–Mg alloys has been investigated in the past [4, 5], also with reference to the effect of minor additions of other elements such as Si, Ag, Sc, Zr [5–12]. Various attempts to establish equilibrium and metastable precipitates in the Al–Cu–Mg–Si system were made but no general agreement was reached [6, 7, 13].

For high-Cu containing Al alloys (copper content higher than 2.5 mass%) with Mg and Si addition, four precipitation sequences are likely to occur

$$\text{SSSS} \rightarrow \text{GPZ} \rightarrow \theta'' \rightarrow \theta' \rightarrow \theta \quad (Al_2Cu)$$

$$\text{SSSS} \rightarrow \text{GPBZ} \rightarrow (\text{S}'') \rightarrow \text{S}' \text{ (semicoherent S)} \rightarrow \text{S (incoherent)} \quad (Al_2CuMg)$$

$$\text{SSSS} \rightarrow \text{GPZ} \rightarrow \beta'' \rightarrow \beta' \rightarrow \beta \quad (Mg_2Si)$$

$$\text{SSSS} \rightarrow \text{QP} \rightarrow \text{QC} \rightarrow \text{Q} \quad [14]$$

where SSSS – supersaturated solid solution, GPZ – Guinier–Preston zones, single-atom layers of Cu on $\{001\}_{Al}$ planes [5], GPBZ – Guinier–Preston-Bagaryastskii zones.

Q-phase is also referred to as h-AlCuMgSi, W- or λ-phase. Its stoichiometry is not well established, but in the past it has been alternatively proposed to be $Al_5Cu_2Mg_8Si_6$, $Al_4CuMg_5Si_4$, $Al_4Cu_2Mg_8Si_7$, $Al_3Cu_2Mg_9Si_7$. It was also suggested [15] that off-stoichiometry of Q-phase could account for the different reported compositions. According to Cayron *et al.* [14], QP, QC are metastable precursors of equilibrium Q-phase. Other authors [15, 16] propose coherent Q'-phase as the only metastable Q-phase precursor. Q'-phase has the same composition as Q and slightly strained structure [15].

According to Chakrabarti and Laughlin Q- and S-phase can not coexist: Q-phase appears in the quaternary system Al–Cu–Mg–Si and replaces S-phase, which is the equilibrium precipitate in Al–Cu–Mg system [7].

The precipitation sequences that take place depend on the actual amount and relative quantity of alloying elements in the SSSS, whose composition is related to the chemical composition of the alloy but could differ from it; this is due to the presence of secondary phases with high temperature stability [6].

* Author for correspondence: paola.bassani@ieni.cnr.it

1388–6150/$20.00

Akadémiai Kiadó, Budapest, Hungary
Springer, Dordrecht, The Netherlands

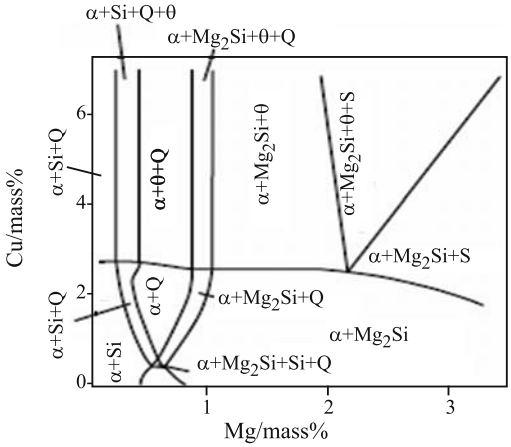

Fig. 1 Isothermal section at 733 K of the Al–Cu–Mg–Si quaternary phase diagram for 0.6 Si [13]

Figure 1 depicts an example of equilibrium phases at 733 K appearing for different composition ranges in Al–Cu–Mg–Si alloys.

A particular focus has to be placed on the precipitation sequence involving θ-phase, since this is the main precipitation sequence occurring in 2xxx series alloys where Cu is the major alloying element. Guinier-Preston zones and particles of each stage undergo reversion (re-solution) before the following phase is formed. While GPZ and θ′′ particles nucleate homogeneously, θ′ and θ form preferentially at dislocation and at grain boundaries respectively. Metastable solubility curves of these precipitates can be represented in a pseudo-phase diagram [17].

According to Eskin [6] in high-copper containing alloys β-phase (Mg_2Si) precipitation could occur when the Mg/Si ratio (mass percent) ranges between 1 and 8, while S-phase forms when Mg/Si>3. These two conditions can also be seen in Fig. 1 for Si= 0.6 mass%.

Silver additions are known to promote the precipitation of Ω phase, nucleating from Mg–Ag co-cluster, in Al–Cu–Mg alloys with Cu/Mg ratio higher than 5 at.% [5, 18]. This precipitate is a slightly distorted form of the equilibrium θ-phase. Yet, small Si additions favours Q phase precipitation, which reduces the available amount of Mg and suppress the nucleation of Ω phase.

Moreover, Si addition is known to enhance hardening response and to reduce the time to peak-hardness. Neither Ω-phase nor β-phase was observed in Al–4Cu–0.3Mg–0.4Ag alloy with systematic Si addition (0.1 to 1.2 mass%) [8].

Zr additions, often together with small amount of Sc, are used to improve the recrystalization resistance of heat-treatable Al-alloys [11, 12] through the formation of Al_3Zr dispersoids, no influence of which is reported on precipitation phenomena.

The present paper provides a thermal analysis of an Al–Cu–Mg–Si alloy with Ag/Zr additions, in three different ageing conditions. Thermal analyses, per se, can not identify the phases involved in the reaction, but with the aid of other techniques (such as optical or electron microscopy, X-ray diffractions) it can be very effective in studying precipitation sequences in heat treatable Al alloys (an excellent overview is provided by Starink [19]).

Experimental

An Al–4.1Cu–0.6Mg–0.5Si alloy with Ag/Zr addition (0.44 and 0.15 mass%, respectively) was water quenched after solution treatment at 505 K/1 h in a muffle furnace. The alloy was then artificially aged at 453 K for soaking time up to 100 h. Vickers microhardness tests (applied load 2.9 N) were performed to characterize the mechanical response to age hardening, and a hardness curve was drawn. When not processed, samples were kept at about 269 K in order to prevent significant natural ageing.

Differential scanning calorimetry analyses were conducted on samples representative of as-quenched, peak-aged (16 h soaking) and overaged (100 h soaking) conditions. Tests were carried out in inert atmosphere (argon), by heating samples from room temperature to 803 K at 5, 10, 20 and 30 K min^{-1}, using a Setaram Labsys TGA/DTA-DSC equipment. Cooling rate was 30 K min^{-1} for every test. Heat flux and temperature calibrations were performed by using pure gold, aluminum and indium fusion enthalpy and melting points respectively. DSC samples were prepared by cutting with a diamond saw and then grinding to their final shape. The mass of each specimen was about 70 mg. Samples were weighted before and after DSC scan. No significant mass increase was observed. Baseline correction was carried out with a pure aluminium sample with approximately the same mass.

For comparison purposes, similar tests were performed on a conventional Al–4.4Cu–0.5Mg–0.9Si–0.8Mn alloy.

Selected samples were polished with conventional metallographic techniques and observed in a scanning electron microscope equipped with EDXS (energy dispersion X-ray spectrometry) probe.

Results

Hardness tests

Hardness curves for Al–4.1Cu–0.6Mg–0.5Si+Ag/Zr alloy and for Al–4.4Cu–0.5Mg–0.9Si–0.8Mn alloy

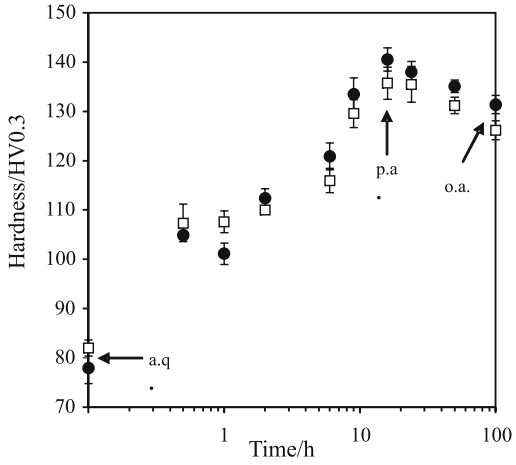

Fig. 2 Hardness curve for ● – Al–4.1Cu–0.6Mg–0.5Si+Ag/Zr and □ – Al–4.4Cu–0.5Mg–0.9Si–0.8Mn alloys aged at 453 K. Arrows and reference codes indicate the ageing condition of samples subjected to DSC analyses

are depicted in Fig. 2. Time to peak hardness is approximately the same for both alloys (16 h) but the Ag/Zr bearing alloy shows a higher maximum hardness (~140 HV *vs*. ~135 HV).

On the basis of these results, three sets of specimens, shown in Fig. 2, were selected to be used for DSC analyses, namely as-quenched (a.q.), peak-aged (p.a., 16 h ageing) and overaged (o.a., 100 h ageing).

DSC analyses

DSC scans performed on as-quenched specimens at different heating rates are summarized in Fig. 3. In this condition, the Ag/Zr bearing alloy shows the complete precipitation sequence. Five exothermic peaks can be observed (upwards in Fig. 3a and labelled as I, II, III, IV and V) at the lowest heating rates (5 and 10 K min^{-1}). At scanning rates of 20 and 30 K min^{-1} some reactions peaks superpose.

A comparison among heat flow curves of as-quenched and aged conditions is presented in Fig. 3b, at scanning rate of 10 K min^{-1}. It clearly appears the general trend for peaks to be less sharp for aged conditions. Further, peaks I (below 473 K) and II (at about 523 K, depending on heating rate) disappear in aged samples, while peak III (at about 573 K) moves towards lower temperature and it is preceded by an endothermic dissolution through. The specific enthalpy involved in the reaction related to peak III decreases with increasing ageing time (Table 1). Peaks IV and V occur at about 623 and 723 K, respectively. An additional endothermic peak, barely visible in as-quenched samples only at the lowest scanning rate (5 K min^{-1}), appears at about 783 K.

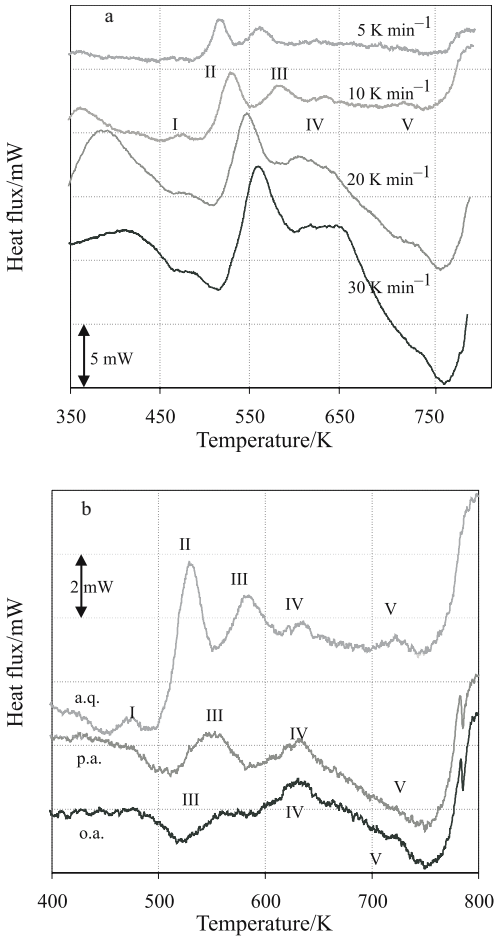

Fig. 3 Heat flow curves during heating of Al–4.1Cu–0.6Mg–0.5Si+Ag/Zr alloy. Curves are shifted along vertical axis for a better visualization. Exothermic peaks (upwards) are labelled I to V. a – as-quenched specimen at different heating rates; b – as-quenched, peak-aged and overaged samples (heating rate: 10 K min^{-1})

Table 1 Variation of specific enthalpy involved in peak III for aged alloys (J g^{-1})

	Heating rate/K min^{-1}			
	5	10	20	30
Peak-aged	–4.35	–3.76	–3.79	–3.10
Overaged	–3.19	–0.96	–1.15	–0.55

Kinetic analysis

Calculation of activation energies was carried out by means of isoconversional Kissinger analysis [19]. Starting from the fundamental kinetic Eq. (1),

$$d\alpha/dt = k(T)f(\alpha) \quad (1)$$

where t, α, $k(T)$, $f(\alpha)$ are time, extent of conversion, rate constant, reaction model, respectively, $k(T)$ is generally replaced by the Arrhenius equation:

$$k(T) = A\exp(-E/RT) \quad (2)$$

where A, E, R are the Arrhenius pre-exponential factor, the activation energy and the gas constant, respectively.

In the case of constant heating rate tests, the following relation can be derived:

$$\ln(T_p^2/\phi) + E/RT_P = \text{constant} \quad (3)$$

where ϕ, T_P are heating rate expressed as K s^{-1}, and peak temperature, respectively. E was obtained by plotting $\ln(T_p^2/\phi)$ *vs.* $1/T$.

The same, modified, procedure was applied considering, instead of T_p, the temperature T_α corresponding to a fixed extent of conversion (α), ranging from 0.1 to 0.9. This procedure was used in order to check possible variations of activation energy over the temperature range for the transformation corresponding to broad peaks.

The analysis was performed on exothermic peaks when possible. As a matter of fact, Kissinger's analysis is applicable when it is possible to define a clear correspondence between transformed fraction and temperature. This correlation is not always well defined, as it happens for example when peaks are broad and their onset and offset are difficult to detect. Furthermore, peaks overlapping should be avoided, since one peak must be related to a single thermal event.

In the present study, for each analysed peak the onset and offset temperature of the reaction were detected on thermograms. The area under each peak was calculated by integration and the temperatures corresponding to fixed values of transformed fraction were found. Plotting this value with respect to temperature can help in understanding whether one or more reactions can be ascribed to the examined peak.

Table 2 summarizes the analyses performed.

The results of peak analyses will be here presented separately for each peak.

Peak I

As shown in Fig. 3a, the identification of peak onset temperature is difficult since it occurs in low temperature region where transient effects are observed.

Table 2 Kinetic analyses performed

	Peaks				
	I	II	III	IV	V
As-quenched	x	✓	–	x	✓
Peak-aged	–	–	✓	x	x
Overaged	–	–	✓	✓	x

✓ – analysed peak, x – unreliable results, – – peak not observed

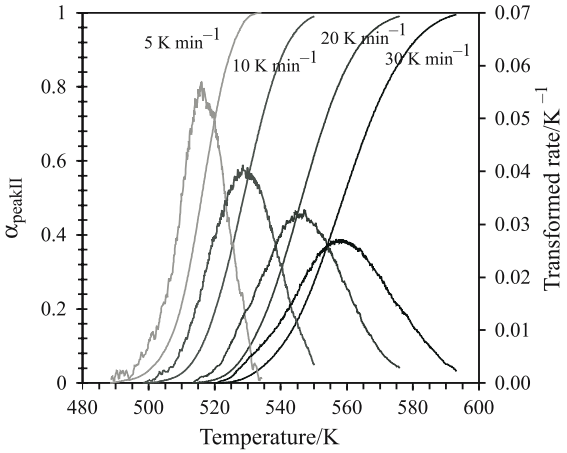

Fig. 4 Transformed fraction and transformation rate for peak II in as-quenched samples for different heating rates

Peak II

This peak occurs only in as-quenched specimens. The evolution of the transformed fraction and the transformation rate are depicted in Fig. 4, showing that no peak overlapping occurs. Activation energy, calculated on the basis of a $\ln(T_\alpha^2/\Phi)$ *vs.* $1000/T_\alpha$ plot (Fig. 5a), decreases with increasing transformed fraction (Fig. 5b), ranging from about 100 to about 75 kJ mol^{-1}.

Peak III

Heat flow curves of as-quenched specimens show this exothermic peak at about 573 K. It occurs at lower temperature for aged alloys (as it clearly appears in Fig. 6). The activation energy, calculated the same way as for peak II, is about 100 kJ mol^{-1} (Fig. 7) for aged specimens, and it is much lower for as-quenched material. The analyses of transformed fraction and transformation rate for as-quenched samples (Fig. 8) suggest a peak superposition that prevents reliable results for Kissinger's analysis.

Peak IV

Reliable values for activation energy related to this reaction could be obtained for this peak only for the overaged samples, where it slightly increases with transformed fraction from 130 to 145 kJ mol^{-1}. Also for this peak the activation energy evolution for as-quenched and peak aged conditions was prevented by difficulties in the identification of onset and offset temperatures.

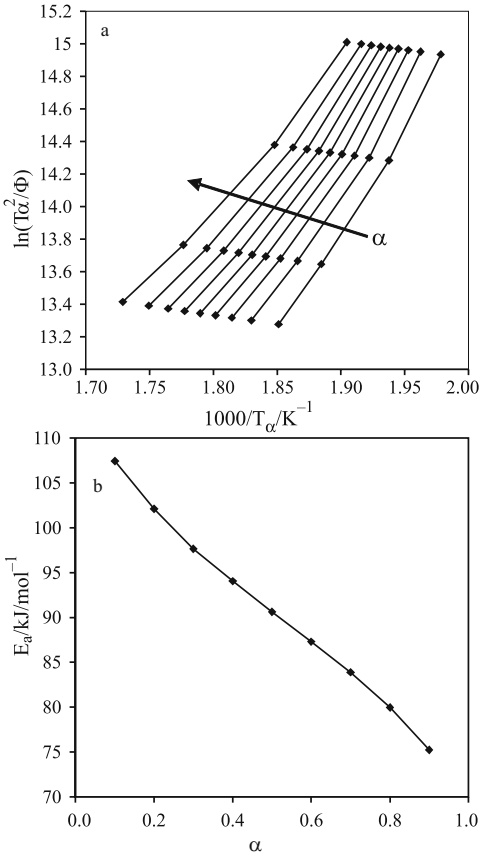

Fig. 5 a – $\ln(T_\alpha^2/\Phi)$ *vs.* $1000/T_\alpha$ plot for activation energy calculation of peak II in as-quenched samples. b – activation energy *vs.* fraction transformed, derived from Kissinger's analyses of the peak, for as-quenched samples

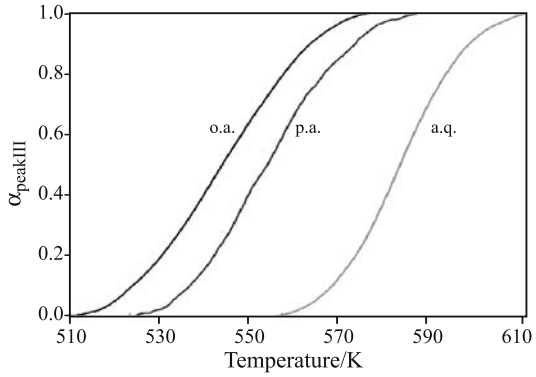

Fig. 6 Peak III transformed fraction *vs*. temperature (heating rate 10 K min^{-1}) for as-quenched (a.q.), peak aged (p.a.) and overaged (o.a.) samples

Peak V

Only the as-quenched alloy shows a clear peak V. Calculation of activation energy provides very high values (about 250 kJ mol^{-1}).

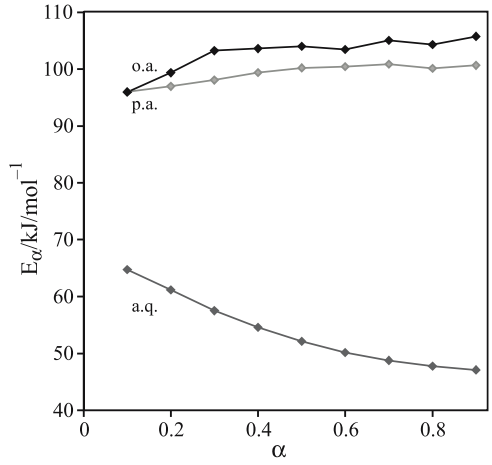

Fig. 7 Peak III activation energy *vs.* transformed fraction for as-quenched (a.q.), peak aged (p.a.) and overaged (o.a.) samples

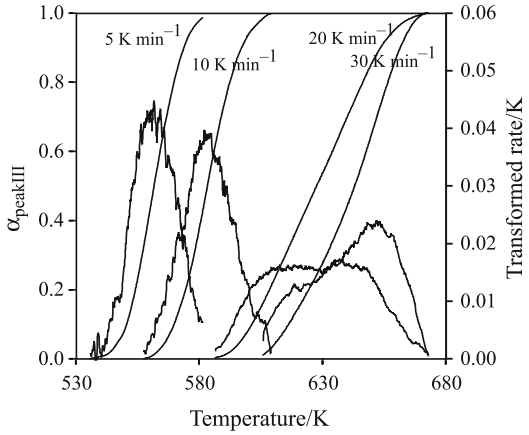

Fig. 8 Transformed fraction and transformation rate for peak III in as-quenched samples for different heating rates. When heating rate exceeds 10 K min^{-1} more than one reaction is reasonably related to this peak

Discussion

On the basis of literature data, phase diagrams and hardness tests, an attempt to identify the precipitation sequence of the investigated Al–4.1Cu–0.6Mg–0.5Si alloy with Ag/Zr additions can be made, considering the set of exothermic peaks observed at increasing temperatures.

Peak I

This exothermic peak takes place in the temperature range slightly higher than that of GPZ solubility for 4%Cu Al-alloys [17]. The hypothesis of GPZ formation can be confirmed noting that aged samples do not show this thermal effect.

Peak II

This exothermic peak can be related to θ′′ precipitation. Also in this case the peak onset is slightly higher than solubility limit for 4%Cu Al-alloys [17], but the heating rate dependence of peak temperatures and the presence of minor amounts of other alloying elements could account for this difference. The assumption can be made also considering that θ′′ precipitates are strenghtening particles [20] and pointing out that this peak does not take place in aged alloys, the reaction having previously occurred during ageing. As depicted in Fig. 5b, activation energy decreases as transformed fraction increases; a similar behaviour was also found by testing a standard Al–4.4Cu–0.5Mg–0.9Si–0.8Mn (Fig. 9). This behaviour could be due to nucleation processes, as already suggested by Starink and Zahra [21].

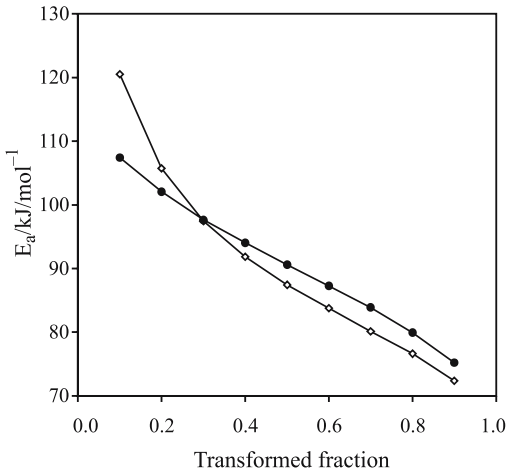

Fig. 9 Activation energy *vs.* transformed fraction for peak II in
• – Al–4.1Cu–0.6Mg–0.5Si+Ag/Zr alloy and
○ – Al–4.4Cu–0.5Mg–0.9Si–0.8Mn alloy

Peak III

Before examining this thermal event, it is worth noting that in the aged alloy it is preceded by an endothermic trough which is deeper for the peak aged condition. This can be due to θ′′-particles dissolution, which are more copious in peak-hardened alloy. Exothermic peak III can thus be related to θ′ precipitation, which locally follows θ′′ dissolution. In the overaged condition, significant fraction of θ′-phase could have formed before DSC scans, and this explains why the released heat (Table 1) is lower than in peak-aged alloy. In this latter case, it is likely that θ′ nucleation had already started during ageing: activation energy is roughly constant with transformed fraction (Fig. 7), and it is similar for both aged conditions.

Peak IV

Peak temperature of this event lies in the temperature range in which precipitation of Q-phase or of its metastable precursors are reported to take place [22, 23].

Peak V

On the basis of Al–Cu phase diagram [17], this exothermic effect is to be related to θ-phase precipitation. Only as-quenched samples show it clearly for each scanning rates, while in aged conditions it is not well-defined. It is suggested that during ageing also copper-containing particles, such as Q phase or its precursors, precipitate, thus reducing the amount of copper available to form θ-phase. Q-phase would remain stable up to about 783 K [13].

Endothermic peak

Literature data [13] suggests that for this group of alloys an endothermic effect is provided at 783 K by the dissolution of quaternary Q-phase. To verify this statement, two aged specimens were heated in a muffle furnace, held at 783 and 788 K for 15 min and rapidly quenched. SEM and EDXS analyses were performed on both specimens. Figure 10 shows a BSE image of the alloy heated at 783 K. EDXS analyses revealed white particles as containing aluminium and copper with Al/Cu ratio close to 2:1 (as θ phase, Al_2Cu). Grey particles, visible in the micrograph, were found to bear aluminium, copper, magnesium and silicon: their presence permits to identify them as quaternary Q-phase. No such phase was found in samples kept at 788 K, thus allowing to indicate the endothermic peak as related to Q-phase dissolution. Further, the shape of the peak suggests the occurrence of an incipient melting, but more optical and electronic microscopy observations are needed to confirm this hypothesis. This fact and the reported stability of Q-phase up to 783 K [13], where the thermal event previously described was observed, led to associate peak IV to Q-phase precipitation.

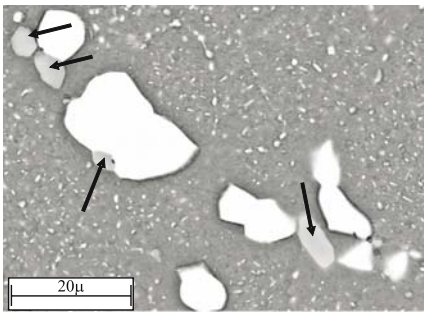

Fig. 10 BSE micrograph of Al–Cu–Mg–Si–Ag/Zr alloy held at 783 K for 15 min. Grey particles (arrowed) are Q-phase precipitates; white particles are θ phase

Conclusions

Hardness tests performed on aged Al–Cu–Mg–Si+Ag/Zr and on conventional Al–4.4Cu–0.5Mg–0.9Si–0.8Mn alloys confirm that the contribution of Ag can enhance mechanical properties more effectively than Si only. Peak hardness is mainly related to the presence of metastable θ′′-phase and of nucleated θ′-phase. The complete dissolution of θ′′ causes a loss in mechanical properties (overaging).

Activation energy for θ′′ precipitation was found to be decreasing with increasing transformed fraction, and the same behaviour is shown by a similar alloy (Al–4.4Cu–0.5Mg–0.9Si–0.8Mn); this can be related to the effect of nucleation processes.

Equilibrium phase precipitation (θ) seems to be reduced in aged alloy. It is suggested that also Cu-rich particles (Q phase) form during ageing, thus reducing the copper content available for θ-precipitation. The presence of Q-phase in aged alloy up to 783 K and its dissolution at 788 K were confirmed by EDXS analyses performed on specimens held at 783 and 788 K, respectively and rapidly cooled.

References

1 I. J. Polmear, 'Light Alloys – Metallurgy of the Light Metals', 3rd Ed., Arnold, London 1994.
2 International standard; EN 515:1993 – Aluminum and Aluminum Alloys – Wrought Products – Temper Designations.
3 J. S. Robinson, R. L. Cudd and J. T. Evans, Mater. Sci. Technol., 19 (2003) 143.
4 J. E. Hatch, 'Aluminum: Properties and Physical Metallurgy', American Society for Metals, Metals Park, OH 1984.
5 S. P. Ringer and K. Hono, Mater. Charact., 44 (2000) 101.
6 D. G. Eskin, J. Mater. Sci., 38 (2003) 279.
7 D. J. Chakrabarti and D. E. Laughlin, Prog. Mater. Sci., 49 (2004) 389.
8 X. Gao, J. F. Nie and B. C. Muddle, Mater. Sci. Forum, 217–222 (1996) 1251.
9 J. Royset and N. Ryum, Int. Mater. Rev., 50 (2005) 19.
10 M. Vedani, G. Angella, P. Bassani, D. Ripamonti and A. Tuissi, J. Therm. Anal. Cal., 87 (2007) 277.
11 Y. W. Riddle and T. H. Sanders, Jr., Metall. Mater. Trans. A, 35A (2004) 341.
12 J. D. Robson, Acta Mater., 52 (2004) 1409.
13 M. J. Lawday, M. R. Clinch, S. J. Harris and B. Noble, Mater. Forum, 28 (2004) 1256.
14 C. Cayron and P. A. Buffat, Acta Mater., 48 (2000) 2639.
15 C. Wolverton, Acta Mater., 49 (2001) 3129.
16 C. Ravi and C. Wolverton, Acta Mater., 52 (2004) 4213.
17 R. W. Cahn and A. L. Greer, Physical Metallurgy, R. W. Cahn and P. Haasen, Eds, 4th Ed., North Holland 1996, p. 1723.
18 S. P. Ringer, K. Hono, I. J. Polmear and T. Sakurai, Acta Mater., 44 (1996) 1883.
19 M. J. Starink, Int. Mater. Rev., 49 (2004) 191.
20 M. F. Ashby and D. R. H. Jones, 'Engineering Materials 2', 2nd Ed., Butterworth-Heinemann, Oxford 1998, p. 100.
21 M. J. Starink and A.-M. Zahra, Mater. Sci. Forum, 217–222 (1996) 795.
22 A. Gaber, K. Matsuda, Z. Yong, T. Kawabata, A. M. Ali and S. Ikeno, Mater. Forum, 28 (2004) 402.
23 P. Bassani, E. Gariboldi and G. Vimercati, J. Therm. Anal. Cal., 87 (2007) 247.

DOI: 10.1007/s10973-007-8376-1